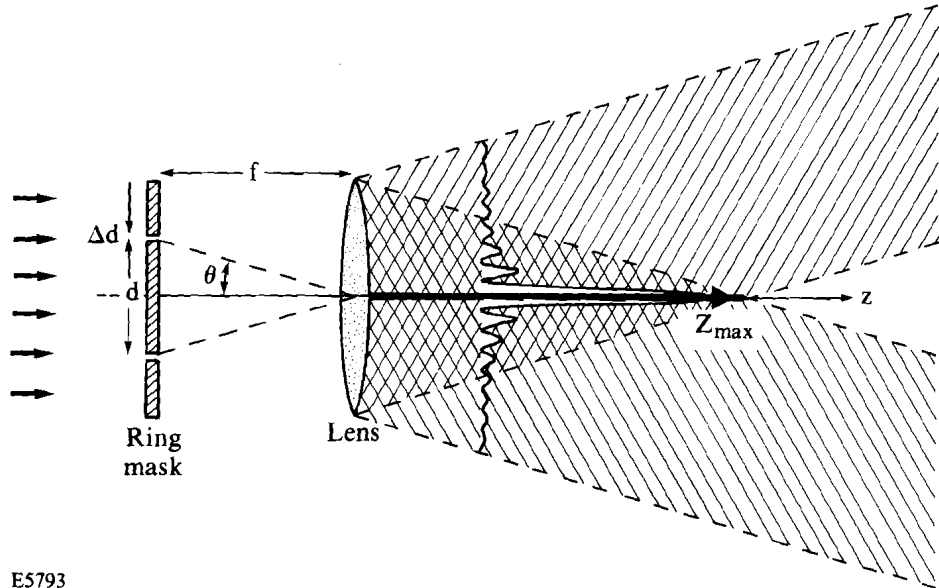# Section 2

ADVANCED TECHNOLOGY
DEVELOPMENTS

2.A Experimental Investigation of Bessel-Beam Characteristics

Previous work by Durnin[1] has shown that the J_0 Bessel function, as an exact solution to the free-space Helmholtz equation, may be of interest in optics. The particular interest in this solution lies in its "diffraction-free" propagation characteristics. That is, the J_0 solution corresponds to the propagation of a very narrow beam (the central portion of the J_0^2 transverse intensity distribution) without transverse spreading over distances exceeding by orders of magnitude the Rayleigh range of Gaussian beams of the same initial FWHM. In the ideal case the electric field of the (zero-order) Bessel beam is given by

$$E\left(r,\phi,z,t\right) = a\ e^{i\left(-\omega t + k_{\parallel}z\right)} J_0\left(k_{\perp}r\right)\ ,$$

where the propagation direction is along z, $k_{\parallel} = (2\pi/\lambda)\cos\theta$, $k_{\perp} = (2\pi/\lambda)\sin\theta$, and θ is a fixed angle to be specified later. However, one should not expect efficient power transport via Bessel beams because of the many side lobes accompanying the central spot.[2-4]

Durnin et al.[2,4,5] have also reported some experimental verifications of these predictions. They used a thin metal ring mask illuminated by a HeNe laser placed in the focal plane of a lens, as shown in Fig. 46.9, to generate a near-ideal Bessel beam. In particular, they showed good agreement between the predicted and the experimentally measured transverse and longitudinal-intensity distributions.

Fig. 46.9
Schematic setup for generating Bessel beams after Durnin et al.[1]

An alternative experimental setup was reported by Turunen et al.,[6] who used a holographic optical element to generate the Bessel beam. These authors reported 10% power conversion between the input power and the power contained in the Bessel beam. While the cross-sectional intensity distribution closely resembles a J_0 beam, the central peak intensity varied rapidly with distance, with a maximum toward the end of the useful focal range.
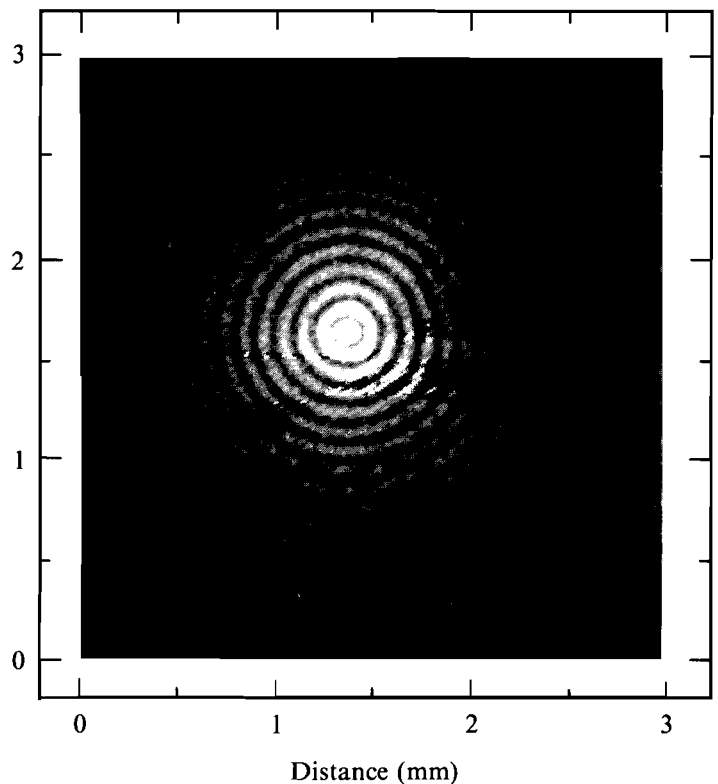
Two alternate schemes for generating long-focal-length beams have been suggested by Indebetouw.[7] One scheme uses a Fabry-Perot interferometer to generate a high-quality ring instead of Durnin's metallic ring mask, and the other scheme uses an axicon (a cone-shaped optical element) illuminated with a collimated beam. While the former leads to basically the same results as Durnin's Bessel-beam generator, the latter leads to increasing on-axis intensity with distance from the axicon because of the increase in geometrical annular area contributing to the intensity on axis. This behavior is completely analogous to that in Turunen's setup.[6]

Several authors[8] have attempted to implement various compromises between the features of Gaussian and Bessel beams. In one recent publication Thewes et al. attempted to optimize the central spot intensity at the expense of the outer ring intensities.[9] However, any such scheme necessarily limits the distance over which the central beam maintains its nondiffractive properties.

In this article we present experimental data at various laser wavelengths and pulse durations to point out some additional characteristics of Bessel beams beyond those reported so far. In particular, we will show interferometric measurements of the phase front of Bessel beams, typical transverse and longitudinal Bessel-beam profiles, and the extent to which they agree or disagree with predictions. We will also present detailed data on energy content in the Bessel rings. Finally, we will demonstrate that unstable resonators are potential Bessel-beam sources under certain conditions. The experimental results will be compared with both the theoretical (ideal) Bessel-beam predictions as well as with computer simulations using the actual experimental parameters.

Experimental Setup and Results

The Bessel-beam generator setup shown in Fig. 46.9 was used for a number of experiments. In Fig. 46.10 we show a typical transverse Bessel-beam profile using a 1.054-μm, Nd:YLF laser source of ~1-ns pulse duration. The annular ring mask was made from a metal-coated glass substrate into which a ring was etched with a 12.5-mm inner diameter and a 0.1-mm ring width. The lens used to generate the Bessel beam was a 1-m focal-length lens.
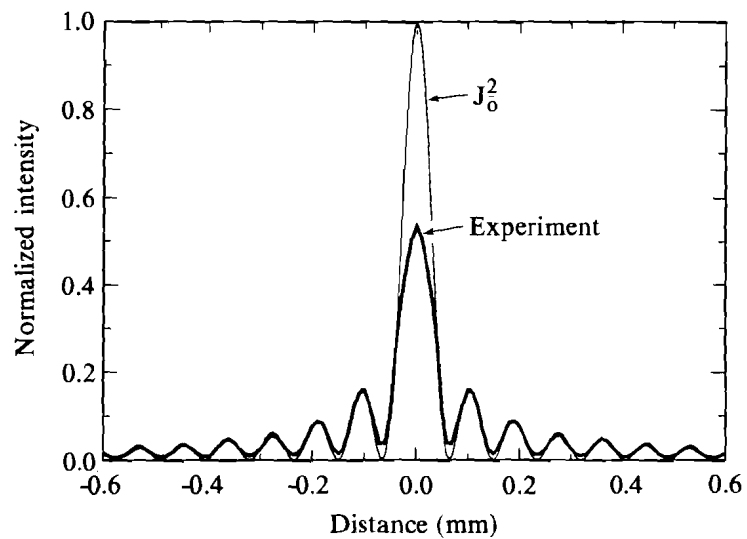

Fig. 46.10
Typical Bessel-beam photograph obtained with a ring aperture of 12.5-mm diameter and 0.1-mm ring width, illuminated by a 1-ns, 1.054-μm, collimated laser pulse from a mode-locked Nd:YLF laser. The photograph is taken at 1 m from the 1-m focal length lens (see Fig. 46.9).

E5794

Bessel-beam photographs were taken at several distances from the lens out to 3.75 m from the lens, well beyond the expected geometrical focal range[1,5] for the Bessel beam of $Z_{max} \approx R/[\tan(d/2f)] \approx 2.8$ m. Here, R is the smaller of either the radius of the lens or the "effective" radius of the diffraction pattern cast onto the lens. The effective radius is defined as $R_{eff} = d/2 + f\lambda/\Delta d$, where d and Δd are the diameter and width of the ring aperture, and f is the focal length of the lens. In the above case the focal range of our Bessel beam was limited by the size of the diffraction pattern on the lens ($R_{eff} \approx 17$ mm), whereas the lens radius was 4 cm.

An azimuthal average about the center of symmetry of the Bessel beam in Fig. 46.10 is shown in Fig. 46.11. Also shown in Fig. 46.11 is a J_0^2 curve normalized to an average of the first six side lobes of the transverse intensity distribution. This normalization was found to be the best one based on arguments presented later in this article. We note the general agreement between the experimental data and the ideal J_0^2 intensity distribution. However, we also note that the central maximum is well below the expected value and that the minima in the distribution are not true zeros.

E5795

Fig. 46.11
Transverse intensity profile of the Bessel beam in Fig. 46.10 obtained from azimuthally averaging the digitized data in Fig. 46.10.

The data was corrected for film response as determined from separate calibration experiments using the same laser pulses and standard procedures.[10] Thus, film response cannot account for the non-zero minima, nor can film halo effects. We also estimate that the errors inherent in azimuthal averaging (mostly the determination of the exact center of symmetry) cannot account for this discrepancy. However, we note that the image in Fig. 46.10

shows considerable speckle that we attribute primarily to light scattered by the etched ring mask. This scattering is most likely the primary cause for the non-zero minima of the observed Bessel beams as well as the reduced center-peak intensity.

The size of the central lobe, i.e., the diameter of the first zero ring ($125\pm5\mu$m), agrees very well with the predictions ($d_{1z} = 4.81/k_\perp \approx 122\ \mu$m). In fact, this good agreement between J_0^2 and experimental transverse intensity distributions holds even well beyond the geometrical focal range Z_{max}, although the overall intensity drops rapidly for $z > Z_{max}$.

From a series of images taken at different distances we have obtained the longitudinal intensity distribution (Fig. 46.12) for the center lobe of the Bessel beam. Figure 46.12 also contains the simulated longitudinal intensity distribution on the basis of numerical Fresnel diffraction simulations. The agreement between experiment and theory is again reasonable. We note that the monotonically decreasing intensity distribution in Fig. 46.12 differs markedly from that shown in Ref. 5 and reproduced in modified form in Fig. 46.13. The difference lies in whether the Bessel-beam propagation at long distances is primarily limited by diffraction from the lens aperture (lens-limited case, Fig. 46.13) or whether it is dominated by the lateral extent of the diffraction pattern from the mask (diffraction-limited case, Fig. 46.12). In the latter case one can think of the lens as being of nearly infinite extent compared to the diffraction pattern cast by the ring aperture.

Figure 46.13 shows the on-axis Bessel-beam intensities for the case where the lens diameter equals the diameter of the ring mask ($R_{lens} = d_{ring} = 12.5$ mm). The three distributions are for different ring widths. Figure 46.13(a) is typical for a lens-limited Bessel beam generated by a narrow ring width (25-μm) casting a diffraction pattern onto the lens that far exceeds the lens dimensions. As the ring width is increased, the on-axis intensity distribution deviates more and more for ideal Bessel-beam propagation [see Figs. 46.13(b) and 46.13(c)]. Also shown in Fig. 46.13 is the on-axis intensity distribution for a Gaussian beam whose initial FWHM at $z = 0$ equals that of the Bessel beam.

When comparing Figs. 46.12 and 46.13 we note that for a lens of given focal length the focal range of Bessel beams is always larger for the diffraction-limited case (Fig. 46.12) than for the lens-limited case (Fig. 46.13). However, in all cases the focal range of the Bessel beams significantly exceeds that of the Gaussian beams of initially equal FWHM.

A characteristic of Bessel beams is that each ring in the pattern carries approximately the same energy (or power). We have verified this prediction in Fig. 46.14 for the Bessel beam shown in Fig. 46.11. The numerical predictions for the ring energies for this particular experimental setup are practically identical to those made on the basis of J_0^2 and basically agree with the experimental data except for a systematic trend in the center-lobe intensity.
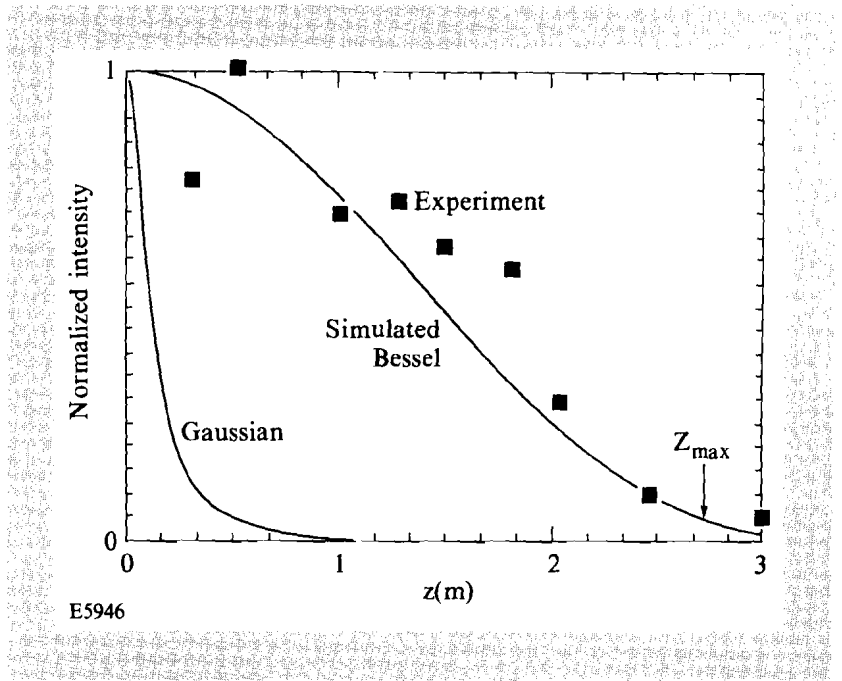
E5946

Fig. 46.12
Intensity distribution of the central Bessel lobe along the direction of propagation for the Bessel beam shown in Fig. 46.11. The intensity at long distances is primarily determined by the limited extent of the diffraction pattern of the ring mask rather than the dimension of the lens. Also shown are the predicted intensity distributions on the basis of Fresnel diffraction calculations and the longitudinal-intensity distribution for a Gaussian beam of equal FWHM at the lens.
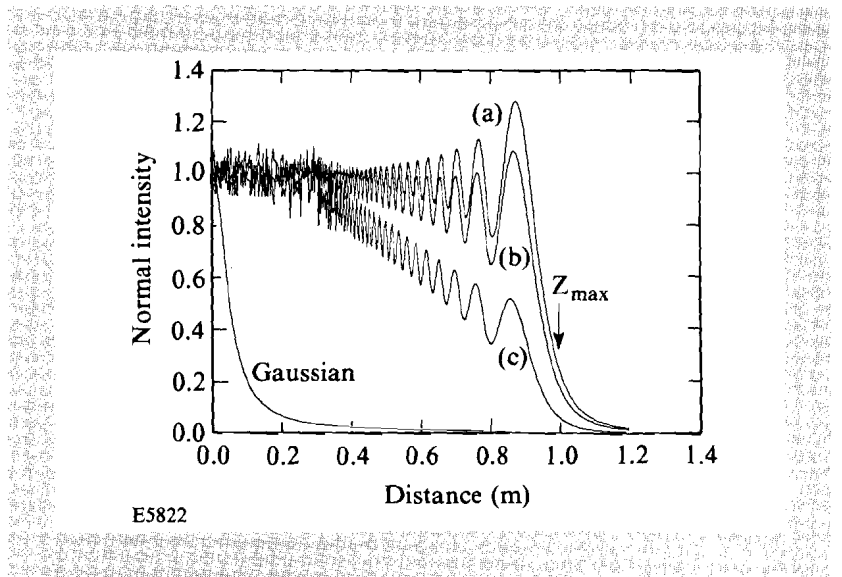

E5822

Fig. 46.13
Longitudinal intensity distribution of the central Bessel lobe for lens-limited Bessel beams where the lens diameter equals the ring radius and a ring width of (a) 25 μm, (b) 50 μm, and (c) 100 μm. The ring diameter is 12.5 mm and focal length of the lens is 1 m.
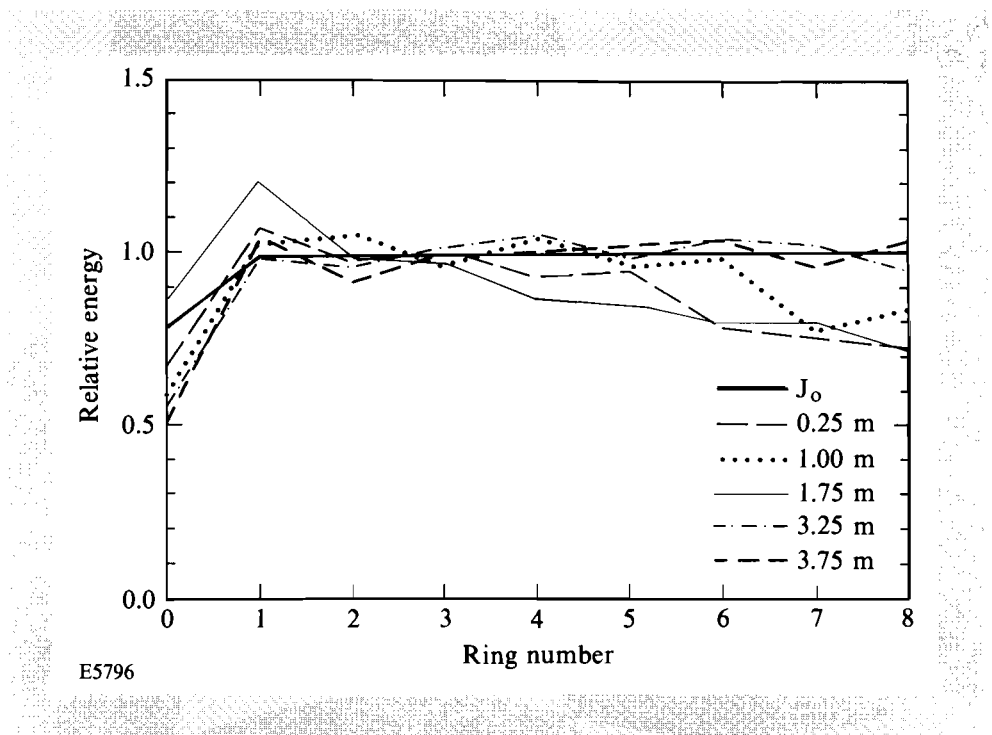
Fig. 46.14
Comparison of theoretical and experimental Bessel-ring energies at various distances along the Bessel-beam propagation. The Bessel beam is the same as that shown in Figs. 46.10–46.13. The systematic deficiency in the experimental energy content of the center lobe is explained by scattering of light at Bessel ring-mask substrate.

There are several potential sources for the low center-lobe intensity. Among them we can rule out film response and saturation, they were accounted for by careful calibration[8] under exactly the same experimental conditions. Similarly, mask asymmetries would have to be so gross as to be easily detected in order to account for the observed decrease in center-lobe intensity. In contrast, scattering within the ring mask with its concomitant phase shifts is expected to significantly reduce the center-lobe intensity, since at the peak of the center lobe all E-fields have to interfere constructively. This condition is fulfilled for the light diffracted from the ring mask, but it is not fulfilled for light scattered by the mask substrate. Consequently, the center-peak intensity can only be decreased by the presence of scattered light.

The regions of zero intensity in the transverse J_0^2 distribution require similarly perfect destructive interference of all the E-fields incident in those regions. Any scattering will invariably lead to non-zero intensities in those regions. However, the zero-intensity regions may also be affected by any mask nonuniformities because of the lack of compensating E-field contributions from different sites on the mask. On the other hand, the maxima of the side lobes, particularly when regarded as azimuthal averages of the intensity distribution, are much less drastically affected. In fact, one can even construct particular cases where the phase shifts associated with the scattered light cancel out to give no net decrease in side-lobe intensity, at least for certain side lobes at certain distances. These arguments therefore justify the normalization of the ideal J_0^2 intensity distributions to an average of the first several side lobes of the experimental intensity distributions (see Fig. 46.11).

An intuitive understanding of Bessel beams is obtained by thinking of a linear combination of plane waves whose wave vectors lie on a cone of opening angle θ. The x-y Fourier transform of the electric-field vector of a Bessel beam is a ring, the same ring that generates the Bessel beam in Fig. 46.9. At the same time, the zero-order Bessel beam can be seen as a plane wave with reduced wave vector $k_{||} = k\cos\theta$, as in Eq. (1). The angle θ is given by $\theta = d/2f$, where d is the ring diameter in Fig. 46.9. Since the E-field has opposite signs on either side of its zero values, this corresponds to a π-phase shift in those regions of the otherwise planar phase front of the Bessel beam. A numerical simulation of an interferogram and its experimental counterpart are shown in Fig. 46.15. The phase jumps in the regions of the J_0^2 minima are clearly seen in this figure. Furthermore, we have investigated the phase front of the center lobe of this beam with high accuracy using spatial-synchronous phase detection[11] and we have found that the phase front was planar within the interferometer resolution of λ/80 rms.
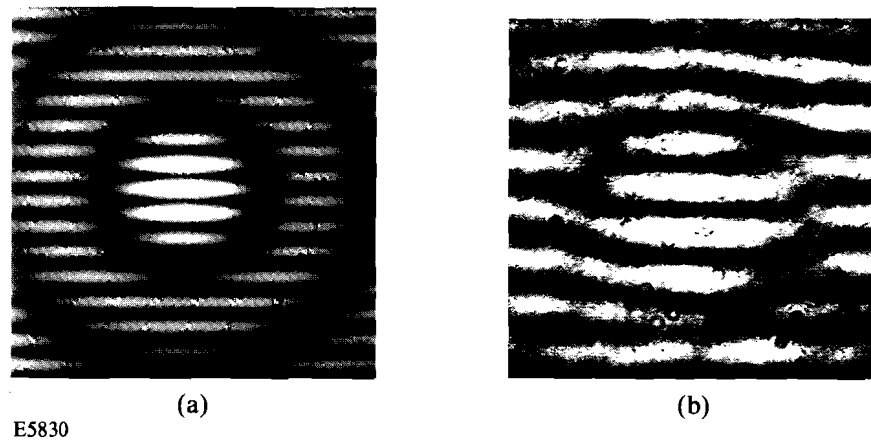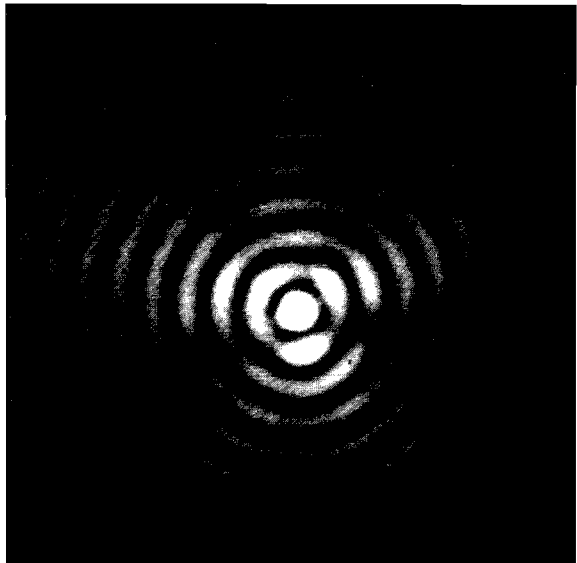

(a)   (b)

E5830

Fig. 46.15
Mach-Zehnder interferograms of Bessel beams. (a) Numerical simulation corresponding to experimental data shown in (b). Note the clearly visible π-phase jumps when crossing the Bessel-beam minima. High-accuracy interferometry of the central spot using spatial-synchronous phase detection has yielded a planar phase front of ≤λ/80 rms.

Two Bessel beams have been generated with the same mask, one at $\lambda_1 = 1.054$ μm (Nd:YLF, pulsed) shown in Fig. 46.10, and the other one at $\lambda_2 = 0.51$ μm (Ar$^+$, cw) shown in Fig. 46.16. The 0.5-μm Bessel beam clearly shows a three-fold asymmetry in the first few rings while no corresponding asymmetry is apparent in the 1-μm image. This distortion was observed to rotate with the mask; furthermore, the same pattern was observed with a second mask, produced at the same time as the first mask. This pattern also persisted if the mask illumination was changed by moving the illuminating beam over the mask. We attribute this distortion to a variation in ring

Fig. 46.16
Transverse intensity distribution of a Bessel beam generated using the same mask as was used for Fig. 46.9 but at $\lambda = 0.51$ μm (cw Ar$^+$). Note that the clearly visible triangular distortion was observed to rotate with the mask. This distortion is attributed to small deviations from uniform mask thickness of the order of a few microns.

E5829

thickness of the mask of a few percent associated with the master pattern that was etched into the gold coating. Unfortunately, this mask error is so small as to be difficult to detect directly; however, blocking part of the ring aperture has been shown to introduce just such intensity asymmetries in the first few side lobes.

Similar asymmetric patterns have been found in numerical modeling of asymmetric ring masks using Babinet's principle by looking at the far-field of a ring mask whose inner disk was placed slightly off-center. With a ring diameter of 12.5 mm and a ring width of 100 μm at a wavelength of 0.5 μm, a 2.5-μm off-center placement of the inner disk clearly accentuates the intensity of the first and second rings on the side opposed to the movement of the inner disk.

Efficient Bessel-beam generation can be obtained with pulsed lasers using an unstable resonator configuration. Such unstable resonators naturally generate ring-shaped beams that loosely approximate the requirements for Bessel-beam generation. An imaging unstable ring-resonator configuration[12,13] is particularly well suited as it images an enlarged version of the scraper mirror onto itself. In practice the sharpness of this image suffers from the finite Fresnel number of the experimental resonator. For this reason we have introduced an additional hard aperture as close to the output as possible in order to reshape the output beam from its original 4.4-mm outer diameter to 3.5 mm; the inner diameter of 2.6 mm remained unchanged. This reduced the output energy by a factor of ~2. However, this Bessel-beam-generation efficiency of ~50% compares very favorably with any of the other experimental values obtained to date. The Bessel beam was then generated with a 7.7-m focal-length lens, which allowed diffraction to fill in the center portion of the beam at the lens. The diameter of the first zero of the Bessel beam was 4 mm and remained unchanged over a distance of ~75 m (see Fig. 46.17). At

the geometrical focal range of ~100 m the Bessel beam was significantly distorted as a result of known phase distortions present in the output beam from the oscillator, although the central spot size was still ~4 mm. A Gaussian beam of the same FWHM would have a depth of focus of twice the Rayleigh range or $2z_R \approx 19$ m. Beyond that distance spreading of the spot is significant whereas the spot size of the Bessel beam remained unchanged over nearly five times that distance. The Gaussian beam would have opened up to a FWHM of ~21 mm at that distance.
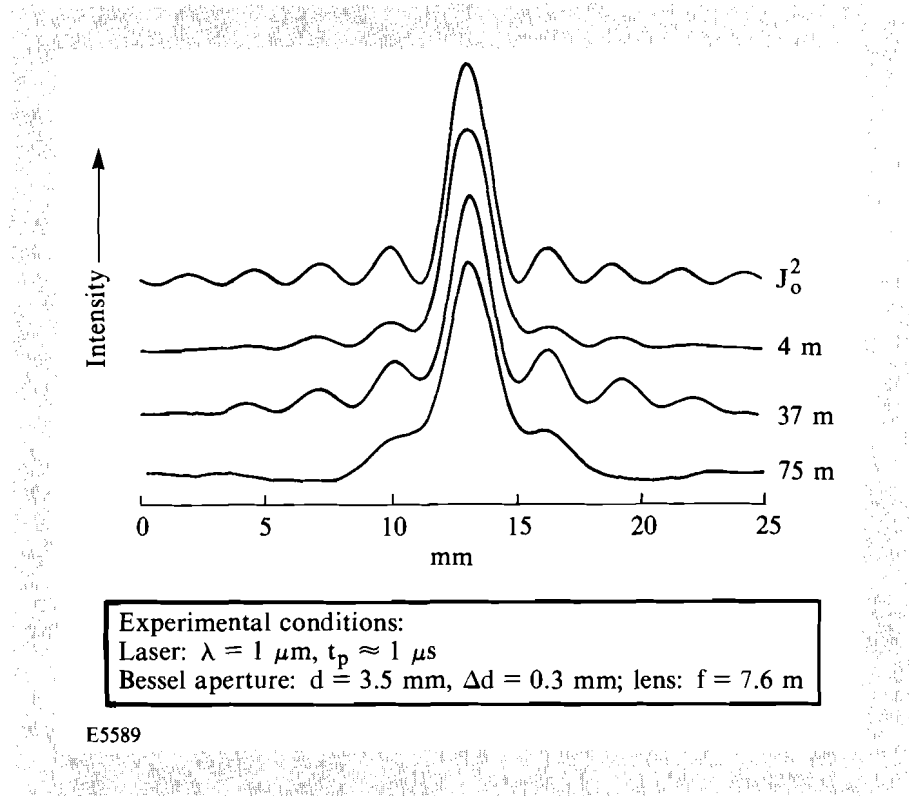

Fig. 46.17
Transverse intensity distribution of Bessel beam generated using the ring-shaped output from an unstable ring Nd:YLF resonator. The J_0^2 distribution shown corresponds to the parameters of the experimental data. The Bessel-beam generation efficiency for this setup is ~50% and could be further improved in an optimized setup.

Conclusions

The size of the central lobe of the Bessel beam as measured by the FWHM of the J_0^2 is typically smaller than either the smallest Gaussian or the smallest Airy disk that can be produced by the same lens. For the purpose of comparison we take a Gaussian with a 1/e-width of its E-field distribution of w_L such that $w_L \approx 3D_{lens}$ resulting in a FWHM in the focal plane of $D_{Gauss} \approx 1.13 f^{\#} \lambda$, where $f^{\#}$ corresponds to the f-number of the lens. The corresponding estimates for the Airy disk are $D_{Airy} \approx 1.01 f^{\#} \lambda$. For the Bessel beam we choose a ring mask of a diameter equal to that of the lens for a setup as shown in Fig. 46.9. The FWHM is then estimated to be $D_{Bessel} \approx 0.70 f^{\#} \lambda$.

While the FWHM of the Bessel beam is clearly the smallest of the three possibilities to generate small spot sizes with a given lens, the peak intensity is smallest for the Bessel beam. On the other hand, the depth of focus, i.e., the length over which neither spot size nor peak intensity changes appreciably, is by far the largest for the Bessel beam.

Thus, for applications where depth of focus and beam definition (spot size) are of prime importance, Bessel beams present significant advantages over Gaussian beams or Airy spots. Such applications certainly encompass long-distance alignment aids or material processing of poorly defined surfaces (machining or direct-write lithographic applications), when laser power is not of prime concern, but beam definition is. Most Bessel-beam applications probably involve nonlinear processes, or detectors or processes with a threshold response.

Our present investigations have shown that good-quality Bessel-beam generation requires avoidance of scattering problems or other phase distortions impressed on the beam by the ring mask in Fig. 46.9 or any equivalent setup (see, e.g., Ref. 5).

Our phase-front measurements of Bessel beams confirm their basic planar-wave character albeit with π-phase jumps between adjacent rings.

High-quality central Bessel spots of predictable intensity can only be obtained for experimental setups that carefully avoid scattering inside the mask. While small imperfections in ring thickness and circularity affect the rings around the central lobe quite strongly (particularly the zero-intensity regions), they affect the central lobe to a lesser degree.

ACKNOWLEDGMENT

REFERENCES

1. J. Durnin, *J. Opt. Soc. Am. A* **4**, 651 (1987).

2. J. Durnin, J. J. Miceli, Jr., and J. H. Eberly, *Opt. Lett.* **13**, 79 (1988).

3. P. Sprangle and B. Hafizi, *Phys. Rev. Lett.* **66** (1991).

4. J. Durnin, J. J. Miceli, Jr., and J. H. Eberly, to appear in *Phys. Rev. Lett.* **66** (1991).

5. J. Durnin, J. J. Miceli, Jr., and J. H. Eberly, *Phys. Rev. Lett.* **58**, 1499 (1987).

6. J. Turunen, A. Vasara, and A. T. Friberg, *Appl. Opt.* **27**, 3959 (1988).

7. G. Indebetouw, *J. Opt. Soc. Am. A* **6**, 150 (1989).